ACS APPLIED MATERIALS & INTERFACES

Research Article

www.acsami.org

Crystallization-Modulated Nanoporous Polymeric Materials with Hierarchical Patterned Surfaces and 3D Interpenetrated Internal Channels

Lijun Ye, Xianchun Shi, Cuicui Ye, Zhouli Chen, Mengmeng Zeng, Jichun You, and Yongjin Li*

College of Materials, Chemistry and Chemical Engineering, Hangzhou Normal University, Hangzhou 310036, People's Republic of China

Supporting Information

ABSTRACT: Poly(oxymethylene)/poly(L-lactic acid) (POM/PLLA) blends are typical melt-miscible binary systems. During isothermal crystallization at various temperatures, in the presence of amorphous PLLA chains, POM crystallizes into banded spherulites with different band spaces, which forms a continuous crystalline phase and serves as a sturdy frame in the final porous materials. On the other hand, the amorphous PLLA chains are simultaneously expelled out from POM crystal lamellae to generate the other continuous phase during the crystallization of POM. Consequently, the interpenetration of the POM lamellae and the amorphous PLLA phase construct a cocontinuous phase structure. All the PLLA constituents are fully included in the interlamellar or interfibrillar of POM crystals. Thus, nanoporous POM materials with hierarchical patterned surface and 3D interpenetrated internal channels have been successfully obtained by extracting the amorphous PLLA phase. It is further found that the POM crystal morphologies in the blends are much dependent on the crystallization conditions. Therefore, the hierarchical patterned structure and the size of internal channels (pore size) can be modulated by adjusting the crystallization conditions.

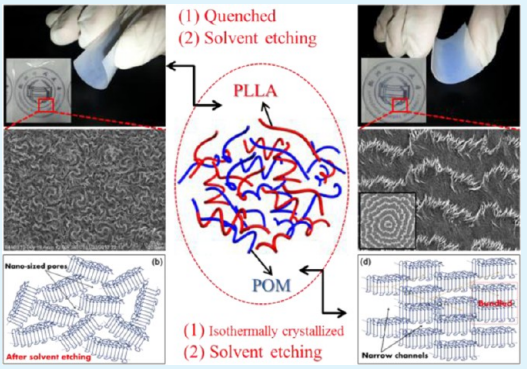

KEYWORDS: *nanoporous polymeric material, hierarchical patterned surface, crystallization, melt-miscible crystalline/crystalline blend*

1. INTRODUCTION

Porous polymeric materials have received tremendous attention and interest due to their potential ability to merge the properties of porous materials and polymers, e.g., low density, high specific surface area and adsorption capacity and uniform and tunable pore size.[1] They can be fabricated either in thin films or in molded monolithic forms and widely applied in gas storage and adsorption,[2−5] separations,[6,7] catalysis,[8,9] drug delivery and controllable release,[10,11] electronic devices,[12,13] even growth templates in the synthesis of nanomaterials with specific shapes[14−16] and many other fields. Three main strategies aimed at fabricating porous polymeric materials have been developed so far. The direct synthesis method is an effective and efficient route to directly generate pores inside the materials by selecting specific reactions during solution polymerization, followed by removal of the solvents retained in the pores.[17−19] The microporous structures with extremely high surface area and the hierarchical porous structures with pore sizes ranging from nanometers to micrometers can be obtained with this strategy. Most different, the direct templating method, known as the "top down" strategy, is essentially a molding or casting technique for the inverse replication of templates with preformed well-defined structures.[20−22] This path, generally, introduces silica nanomaterials (nanoparticles or mesoporous silica), anodic aluminum oxide (AAO), polystyrene (PS) or other polymer nanomaterials as sacrificial materials (templates), scaling down the pore size to the nanometer range just by simple physical or chemical processes, e.g., adsorption and infiltration, layer-by-layer assembly or in situ polymerizations. Moreover, block self-assembly of copolymers (BCPs) has been exploited to make mesoporous or macroporous polymeric materials, especially those with long-term ordered structures, for 2 or 3 decades.[23−25] The approach based upon self-assembly of BCPs is also named as the "soft template" or "bottom up" strategy, by which the nanoporous polymeric materials are obtained via etching or dissolving a block segment of block copolymers with a well-defined ordered structure due to the microphase separation of the thermodynamic incompatible blocks. A distinct but related strategy of preparing macroporous polymeric materials is based on phase separation of binary blends, in which the two components are thermodynamic incompatible. With removal of one of the phases, the residue materials will form a highly interconnected porous network with an inherently high specific surface area.

Received: January 29, 2015
Accepted: March 16, 2015
Published: March 16, 2015

DOI: 10.1021/acsami.5b00848
ACS Appl. Mater. Interfaces 2015, 7, 6946−6954

Favis et al. blended PS with PLLA, forming a cocontinuous structure, where each phase is highly continuous in three dimensions.[26] On removal of the PS component, they obtained highly porous PLLA monoliths, which are proved to have substantial potential for medical and biological applications.[27,28] Upon addition of the PS-*b*-PLLA copolymer as a compatibilizer, the pore size of the obtained PLLA materials decreased drastically from 1.8 to 0.9 μm while that sharply increased to 72 μm by an annealing process. Obviously, several drawbacks are inevitable in adopting such a strategy. Generally, the pores obtained are usually in micrometer-scale due to the thermodynamic immiscibility of the components. And the highly cocontinuous structures are only obtained over very limited blending ratios, and further, porosity of the obtained materials is also narrowly confined. Finally, the cocontinuous structure generated by phase separation of immiscible blends is usually unstable on thermal annealing or exposure to mechanical shear, resulting in inhomogeneity in the pore structure.

The melt-miscible binary blends that contained at least one crystallizable component demonstrates varieties of phase morphologies depending intensively on the miscibility, blending compositions and the crystallization conditions.[29,30] At a given crystallization temperature (T_c), the crystallizable (or high-T_c) component crystallizes while the noncrystallizable (or low-T_c) one still remains amorphous and acts as diluents. Consequently, the noncrystallizable (or low-T_c) component might locate in the interlamellar, interfibrillar and interspherulitic regimes of the pre-existed framework of the crystallizable (or high-T_c) one, depending on the crystallization temperature and blending ratios.[31−34] Banded spherulites are universally observed in many crystalline polymers, especially in miscible binary systems.[35,36] The spherulites that exhibit extinction bands or concentric rings under polarized light microscopy (PLM) are generally postulated to arise from the cooperative twisting of radiating lamellar crystals along their fastest growth directions. The mechanism for lamellar twisting is generally considered originating from the accumulation of stress at lamellar surfaces. In binary blends, the development of surficial stresses might be controlled strongly by the expulsion of the amorphous (or low-T_c) component near the fold surfaces during crystallization of the crystallizable (or high-T_c) one.

A melt-miscible polymer blend containing a crystallizable component, as we considered, is feasible to fabricate nanoporous polymeric materials by selectively etching the noncrystallizable (or low-T_c) components. The amorphous (or low-T_c) component is simultaneously expelled out from the crystal lamellae during the crystallization of the crystallizable (or high T_c) one. Therefore, 3D interpenetrated networks form with the crystal lamellae and the amorphous component between the lamellae. By simply removing of the amorphous (or low T_c) component located between the lamellae, the residue materials will be transformed into perfect 3D porous materials. Two prerequisites are important for the fabrication of such novel nanoporous materials. On the one hand, the segregation of the noncrystallizable (or low-T_c) components should be small enough to make the nanosized pores. In other words, only interlamellar or interfibrillar including structures is feasible for such purpose. It is highly possible that the interspherulitic filling structure leads to the big pore and results in the discontinuity of the crystalline part. On the other hand, the crystallizable (or high T_c) components that should have high crystallinity with few amorphous chains are mixed with noncrystallizable (or low T_c) ones located in the interlamellar and/or interfibrillar regions, so that the almost complete extraction of the latter is easily achieved.

In this work, the crystallization behaviors of melt-miscible POM/PLLA blends have been investigated and the novel porous POM materials are fabricated for the first time. POM crystallizes into the banded-spherulitic frameworks with the PLLA fully included in the space between POM lamellae and/or crystal fibrils. Novel porous POM materials with hierarchical patterned surfaces and 3D interpenetrated internal channels are therefore successfully achieved by selectively removing the PLLA phase. The structure of the nanoporous POM materials can be manipulated by controlling the crystal morphology of the precursor POM/PLLA blends.

2. EXPERIMENTAL SECTION

2.1. Materials. The PLLA (3001D) material used is purchased from Nature Works Co. LLC (USA). The M_n and M_w/M_n are reported to be 89 300 ± 1000 g/mol and 1.77 ± 0.02, respectively.[37] The material contained 1.6% of D-lactide. The POM (MC90) samples are kindly provided by Shenhua Co., Ltd., China. The melt flow index is 9.23 g/10 min. The M_w and M_w/M_n of the POM sample are M_w = 174 300 g/mol and 2.19.

2.2. Sample Preparation. Prior to use, all samples are dried in a vacuum oven at 80 °C for 12 h. PLLA and POM are blended at 190 °C using a batch mixer (Haake Polylab QC) with a twin screw at an initial rotation speed of 20 rpm for 1 min and subsequently raised to 50 rpm for 5 min. All the samples prepared are hot-pressed first at 190 °C under a 14 MPa pressure for 3 min to a film with a thickness of 300 μm, followed by a rapid cooling process (quenched) or isothermal crystallization and then quenched to room temperature. The samples with the thickness of 100 μm for mercury injection testing use the same process, whereas those with the thickness of about 10 μm for PLM and AFM observations are prepared by spin-coating.

Extractions are performed in a Soxhlet extraction apparatus. The PLLA components are extracted with chloroform and, therefore, can as well be referred to as the porogen phase. The temperature of the chloroform in the Soxhlet extraction apparatus is about 60 °C. Following the extractions, all the samples are dried in a vacuum oven at 40 °C. Note that extractions are repeated until the dried extracted specimens achieved constant weight. The obtained films are used for the following characterization.

2.3. Structural Characterization. The optical images of samples are taken by polarizing light microscopy (PLM, Olympus BX51) with equipment of a digital camera. All the samples are spin-coated on a slice of glass, and the temperature is controlled by a Linkam LTS 350 hot stage. The samples are prepared by heating at 190 °C and held for 10 min, and then quenched to the desired crystallization temperatures.

The crystallization behaviors of samples are measured in a differential scanning calorimetry (DSC Q2000) under nitrogen flow at a heating rate of 10 °C/min from 10 to 200 °C, and then held for 5 min to erase the thermal history before being cooled down to 10 °C in a cooling rate of 10 °C/min. The heating and cooling DSC traces are recorded. Before sample scanning, the heat flow and temperature of the instrument are calibrated with sapphires and pure indium, respectively.

Morphology of the blends is observed by field-emission scanning electron microscopy (FESEM). A Hitachi S-4800 SEM system is used for SEM measurements at an accelerating voltage of 2 kV. All the samples are fractured after immersion in liquid nitrogen for about 15 min. The thin films with the thickness of about 100 nm are prepared by spin-coating 8 wt % hexafluoroisopropanol solution onto a glass surface, and are then directly observed under atomic force microscopy (AFM, Nanoscope III MultiMode). Both height and phase images are recorded simultaneously with tapping-mode. Typical values for the RMS amplitude and the set-point amplitude ratio (r_{sp} is defined as the ratio of the cantilever's oscillating amplitude to its freely oscillating amplitude) are 2.0 and 0.7−0.9 V. The amplitude of the freely

DOI: 10.1021/acsami.5b00848
ACS Appl. Mater. Interfaces 2015, 7, 6946−6954

oscillating cantilever is approximately 40 nm. TESP tips with a resonance frequency of approximately 300 kHz and a spring constant of about 30 N/m are used.

A mercury intrusion porosimetry (Micromeritics Poresizer 9320) is employed to measure the surface area and the porosity of the extracted samples. The experimental data treatment is based on the Washburn equation:[38]

$$P_r = -2\sigma_m \cos\theta$$

Where P is the applied pressure, r is the radius of the pore, σ_m is the surface tension of the mercury and θ is the contact angle between the polymer and mercury (480 mN/m and 140° are used for all measurements, respectively). This method can provide the number-average diameter (by the volume/surface ratio), the volume-average diameter, and the pore-size distribution.

3. RESULTS

3.1. Miscibility and Crystallization Behaviors of POM/PLLA Blends. In previous works, we have demonstrated that the POM/PLLA blends exhibited typical lower critical solution temperature (LCST) phase behaviors.[39] PLLA and POM are fully miscible in the melt state at low temperatures due to the weak interaction between the CH_2 groups of POM and the CO groups of PLLA. Although both POM and PLLA are crystalline polymers, PLLA has a much lower crystallization rate than POM. No crystal diffraction peaks for PLLA crystals are observed for the all blend samples when first isothermally crystallized at 141 °C and following quenched to room temperature, as determined by the WAXD pattern (Figure S1 of the Supporting Information). The crystallization rate of POM is fast, and two crystal diffraction peaks at 2θ = 22.7° and 34.8° in the WAXD pattern are observed for all the POM/PLLA blends, which are, respectively, corresponding to the (100) and (105) lattice planes of POM hexagonal crystals, similar to those for the neat POM.[40] At the same time, no diffraction peaks are observed for PLLA crystals, indicating that the PLLA keeps amorphous state and POM is well crystallized. An even higher crystallinity of POM in the blends than that in the neat POM is observed (Table S1 of the Supporting Information) by the thermal analysis, implying that few amorphous segments of POM chains are mixed with the amorphous PLLA chains into the interlamellar and/or interfibrillar areas.

3.2. Crystal Morphologies of POM/PLLA Blends under Different Crystallization Conditions. The formation of spherulites with regular radical banding is generally attributed to the cooperatively twisting of lamellae along their growth directions.[41−46] Many proposals and hypotheses of the mechanisms for such lamellar twisting have been developed.[47−52] It appears very likely that all the mechanisms are based on unbalanced surface stresses leading to the lamellae twisting in polymers or polymer blends. With the incorporation of amorphous PLLA chains, POM tends to form a banded-spherulitic texture, as shown in Figure 1. Banded spherulites of POM with globular and regular shapes are distinctly observed and the space of bands increases but the regularity of bands is depressed with the elevating of crystallization temperature of POM ($T_{c,POM}$). Generally, lamellae helically grow with simultaneous branching from the crystallization center and finally assemble into banded spherulites. The T_c is considered as a main factor to affect the ability of lamellae's twisting and branching. Thus, the increasing of band spaces might be ascribed to falling of the twisting ability of the thickened lamellae upon the elevating of the $T_{c,POM}$. And the period of twisting is proved to be proportional to the square of lamellar thickness by Okano.[53] Moreover, the depression of the branching (screw-dislocating) due to the elevated T_c enlarges the amplitude ratio-phase difference of lamellae's twisting, giving a rise to the reduction of the bands' regularity due to the extended discrepancy of the twisted growth between the adjacent lamellae, as also observed in Figure 1.[54]

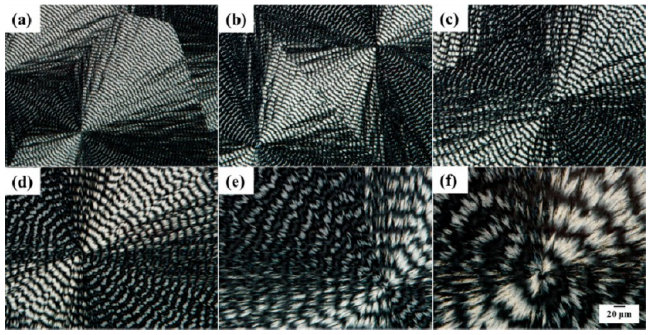

Figure 1. PLM images of POM/PLLA (50/50) samples isothermally crystallized at (a) 141 °C, (b) 143 °C, (c) 145 °C, (d) 147 °C, (e) 149 °C and (f) 151 °C.

3.3. Full Inclusion of PLLA between POM Lamellae in the POM/PLLA Blends. Melt-miscible binary polymer blends containing at least one crystallizable component exhibit a variety of phase morphologies depending on the segregation distance of the components. Liu and Jungnickel[30] have summarized some novel morphologies and kinetics about the crystalline/crystalline miscible systems, i.e., side-by-side, interpenetrating, interlocking and interfiling spherulitic crystallization of the components. Most recently, Han et al. demonstrated the confined nucleation and growth of poly(ethylene oxide) (PEO) on the different crystalline morphology of poly(butylene succinate) (PBS) tuned by various T_c.[36] Actually, when POM crystallizes under various conditions, the POM/PLLA blends can be considered as crystalline/amorphous systems because the PLLA are all in amorphous state in this work and PLLA chains just act as diluents. During isothermal crystallization, all the POM spherulites crystallized at indicated T_c's exhibit globular and regular shapes and occupy the whole space of the initial melts (that is, no PLLA-rich melts are found in Figure 1), indicating that the amorphous PLLA chains are probably mostly included in the POM spherulites (even when the content of PLLA increases to 80%, as shown in Figure S2 of the Supporting Information).

It is, moreover, interesting to find that the amorphous PLLA chains are still fully included in the POM spherulites, though POM crystallizes at a relatively high temperature. It might be ascribed to the depression of the diffusion ability of the amorphous PLLA chains (from the mixed melts) due to their good interactions with POM chains (hydrogen-bonding interactions between the CH_2 groups of POM and the CO groups of PLLA[39]). Furthermore, the globular and regular shapes of the POM spherulites are still observed even POM crystallizes at low temperatures, which are vital different from the "dendritic growth", as reported in some previous literature.[30,55−57] It implied that the amorphous PLLA chains are moderately excluded out from the lamellae, resulting in a nanoscaled interlamellar and/or interfibrillar including of PLLA chains (relatively small portion) due to the good interactions between these two components. Following the crystallization of POM at various $T_{c,POM}$ values, to further certify the vital small

DOI: 10.1021/acsami.5b00848
ACS Appl. Mater. Interfaces 2015, 7, 6946−6954

magnitude interlamellar and/or interfibrillar inclusion of PLLA chains, all the blends are subsequently quenched to 100 °C for the isothermal crystallization of PLLA. Note that the morphologies of POM spherulites, as shown in Figure 2, are

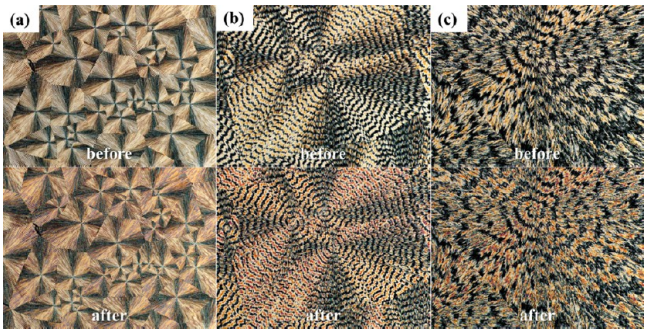

Figure 2. PLM images of POM/PLLA (50/50) blends before and after crystallizing at 100 °C. Note that POM has already crystallized at various $T_{c,POM}$: (a) 141 °C; (b) 147 °C; (c) 151 °C.

essentially the same after the complete crystallization of PLLA compared to the initial ones, indicating that the crystallization of PLLA is confined within the banded POM spherulites (Figure S3 of the Supporting Information). Restricted and limited strongly by the pre-existed POM banded-spherulitic frameworks, PLLA chains could only form some relatively tiny lamellae in the interlamellar and/or interfibrillar areas without causing morphological changes of POM spherulites.

For the quenched samples, however, the globular and regular spherulites cannot be well developed due to the rapid cooling rate. The POM components in the POM/PLLA blends randomly crystallize to form a single lamella and/or crystal stacks (fibrils) and connect eventually to generate a continuous phase upon further growth of the initial lamellae and/or crystal stacks. Meanwhile, the amorphous PLLA chains are also excluded out from the POM lamellae, locating into the regimes between the POM lamellae and/or crystal stacks, to yield the other continuous phase. With the increasing content of PLLA components, the long periods of POM crystals are found to rise gradually, as confirmed by the SAXS pattern (Figure 3). The

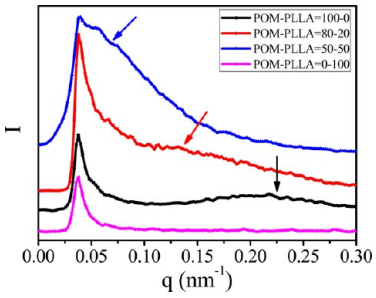

Figure 3. $I-q$ curves collected by SAXS of the quenched POM/PLLA blends.

peaks for POM in the POM/PLLA blends appear to be wide-ranging with the increasing content of PLLA. It is attributed to the wide distributions of the long periods of POM crystals due to interlamellar and/or interfibrillar inclusion of amorphous PLLA chains in the POM/PLLA blends, especially being rapidly quenched from the melt state. This again indicates the full inclusion of PLLA chains into the POM frameworks consisted of crystals to form interlamellar and/or interfibrillar structure.

3.4. Nanoporous POM Materials Obtained from the Crystallized POM/PLLA Blends. Favis et al. have successfully fabricated porous PLLA monolithic materials by etching of the PS components within PS/PLLA blends where phase separation occurred due to the thermodynamic immiscibility. Similarly, we have obtained a novel cocontinuous structure with POM crystals as the frames and amorphous PLLA located between the POM lamellae/fibrils. Such a structure has great potential as a unique template to fabricate meso-/macroporous polymeric materials. The vital small magnitude of interlamellar and/or interfibrillar inclusion of amorphous PLLA chains within POM crystals may essentially endow the final materials with nanostructures. Moreover, the high crystallinity of POM will make the amorphous PLLA chain excluded out from lamellae to be much neater due to the fewer contact with amorphous segments of POM chains, so as to be more thoroughly removed in the further extractions. To further obtain porous monolithic materials from the crystallized POM/PLLA blends, as Favis et al. did, all the samples are carried out with Soxhlet extracting experiments by chloroform.

Figure 4 shows the SEM images of the top and fracture surfaces of POM/PLLA (50/50) blends crystallized under

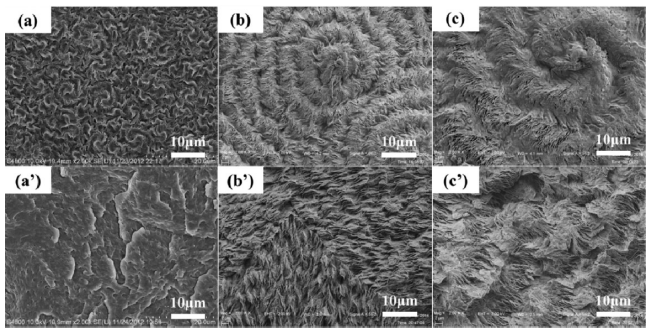

Figure 4. SEM images of top and facture surfaces (fractured on the film thickness direction) of the PLLA-etched POM/PLLA (50/50) blends. The samples obtained from (a, a′) the quenched, (b, b′) 141 °C and (c, c′) 151 °C-isothermally crystallized POM/PLLA (50/50) blend.

various conditions. The top surfaces of the isothermally crystallization samples after the etching of the amorphous PLLA chains are shown in Figure 4b,c. It is obvious that the residue materials after PLLA extraction not only maintained the POM banded-spherulitic texture, but numerous narrow channels are found to regularly and orderly disperse into the bands of POM spherulites. Most interestingly, the distribution of the queues of these narrow channels exhibits identical periodicity to that found with the banded spherulites (as shown in Figure 1), and further generates the hierarchical patterned surfaces of the etched materials. The bands with queues of narrow channels, as we supposed, are corresponding to the "edge-on" lamellae of POM spherulites after removal of the amorphous PLLA chains which are initially included in the interlamellar and/or interfibrillar regimes, whereas those without channels' dispersing are generated by the "flat-to" lamellae (as confirmed by AFM, Figure S4 of the Supporting Information). Figure 4b′,c′ shows the fracture surfaces which exhibit the internal microstructure of the extracted materials. The regular and ordered queues of narrow channels can be

DOI: 10.1021/acsami.5b00848
ACS Appl. Mater. Interfaces 2015, 7, 6946−6954

found inside the residue materials as well. After a simple calculation based on gravimetric method, it is, moreover, interesting to find that almost all the PLLA in the crystallized POM/PLLA blends can be removed by the Soxhlet extraction while the extracted solution contains only PLLA and the film after the extraction only contain neat POM (as evidenced by the FTIR measurements in Figure S5 of the Supporting Information). Associated with the results of gravimetric calculation, it is obvious to conclude that the channels are interpenetrated to yield a 3D network, so as to the almost complete extraction of the amorphous PLLA chains (highly continuous phase) by a simple solvent etching.

For quenched POM/PLLA samples, many irregular holes are found to randomly disperse in the residue materials of the quenched samples after etching by chloroform (Figure 4a and Figure 5). It is obvious that the holes observed are

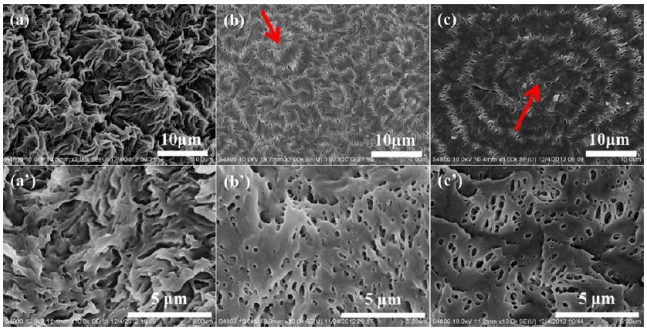

Figure 5. SEM images of top and facture surfaces (fractured on the film thickness direction) of the quenched POM/PLLA blends with the indicated compositions after etching, respectively. (a, a′) POM/PLLA = 20/80; (b, b′) POM/PLLA = 60/40; (c, c′) POM/PLLA = 80/20.

corresponding to the amorphous PLLA phase because chloroform is a good extracting solvent for PLLA, but a nonsolvent for POM. Although, no well-developed POM spherulites are obtained for the quenched samples, the POM/PLLA blends with the compositions ranging from 80/20 to 20/80 can transform into porous POM materials with various pore structures after etching. Moreover, a high content of POM leads to an enhanced trend of the formation of an irregular spherulitic texture (Figure 5). It is further found that all the residue materials can self-support to maintain the original shape, indicating that both PLLA and POM form high-continuity phases to yield a cocontinuous structure in the crystallized POM/PLLA samples.

The surface topographies of a spherulite before and after solvent etching in the POM/PLLA (50/50) samples, in which POM has completely crystallized at different T_c, are further observed with AFM. According to the differences in height, regularly and periodically banded "peak-and-valley" (due to the alternative "flat-to and edge-on" lamellar growth[58]) patterns are found along the radical directions of POM spherulites (Figure 6). For the POM/PLLA (50/50) blend in which POM has crystallized at 141 °C, the height difference, on average, between "peaks" and "valleys" increased drastically from about 70 to 500 nm after solvent etching, as revealed by cross section analysis. Such an increase in height again indicates that the etched amorphous PLLA chains are initially located on the surface of the POM "flat-on" lamellae. PLLA between the "flat-on" lamellae is etched to form "flat-on" nanochannels. These channels are connected with the "edge-on" channels to construct fully 3D interconnected pores in the frame of POM.

Figure 7 shows the macroscopic images of the porous films obtained from the POM/PLLA (50/50) blend in which POM is quenched and isothermally crystallized at 141 °C, respectively. All the obtained films containing water exhibit nice transparency and favorable mechanical properties. It is, moreover, interesting to find that all the porous films, while containing water inside, shine faint but noticeable blue light. Such a phenomenon of interest might be ascribed to the scattering of light (with wavelength ranging from 420 to 500 nm) on the surface of the obtained porous films. Furthermore, the hierarchical patterned surface of the 141 °C-isothermally crystallized samples might enhance the scattering of blue light (as confirmed by UV−vis measurements in Figure S6 of the Supporting Information). To further verify the formation of internal 3D interpenetrating channels, all the crystallized POM/PLLA (50/50) blends have been made into thin films and used for filtration tests after etching. It is found that all the porous films obtained could be used as filtration "papers" and water can continuously flow through the filtration equipment (a water flow of more than 30 L/m^2/h is measured by the water flux testing under 0.3 MPa). Amazingly, a glass of muddy water is transformed into a much clearer one by passing through the porous film obtained from the crystallized POM/PLLA blends, as shown in Figure 8. The porous POM films exhibit a great potential for applications of the sewage treatment, and further, again indicates the 3D interconnected porous structure of the films.

Figure 9 shows the pore-size distributions of the porous materials obtained from the POM/PLLA (50/50) blends under different crystallization conditions (see Table S2 of the Supporting Information for more details). The pore size of the porous materials obtained ranges on a nanoscale. It is, moreover, interesting to find that the pore size of the obtained nanoporous POM materials can by modulated by the crystallization conditions. And the mean pore size of the nanoporous POM materials obtained from the isothermally crystallized POM/PLLA blends increases with the elevating temperature of $T_{c,POM}$. Furthermore, the 3D interpenetrated internal channels, especially the hierarchical patterned surfaces originated from the initial banded-spherulitic frameworks, endow the nanoporous POM materials with hydrophilcity (Figure S7 of the Supporting Information).

4. DISCUSSION

From the above, we have successfully fabricated a novel nanoporous POM material with hierarchical patterned surfaces and 3D interpenetrated internal channels. The pore structure of the final materials can be modulated by controlling the crystal morphology of POM crystallized under various conditions. No well-developed POM spherulites will form during the quenching process. As illustrated in Scheme 1a, single lamellae and crystal stacks of POM connect eventually to weave a self-supporting framework and template the simultaneous formation of a reversed network consisted of the amorphous PLLA chains. As a consequence, the nanoporous POM materials with 3D interpenetrated channels are obtained by removal of the amorphous PLLA chains located in the interlamellar and/or interfibrillar areas of POM crystals (Scheme 1b). During the isothermal crystallization of POM, globular and regular banded spherulites form and develop with the full including of amorphous PLLA chains at various $T_{c,POM}$

DOI: 10.1021/acsami.5b00848
ACS Appl. Mater. Interfaces 2015, 7, 6946−6954

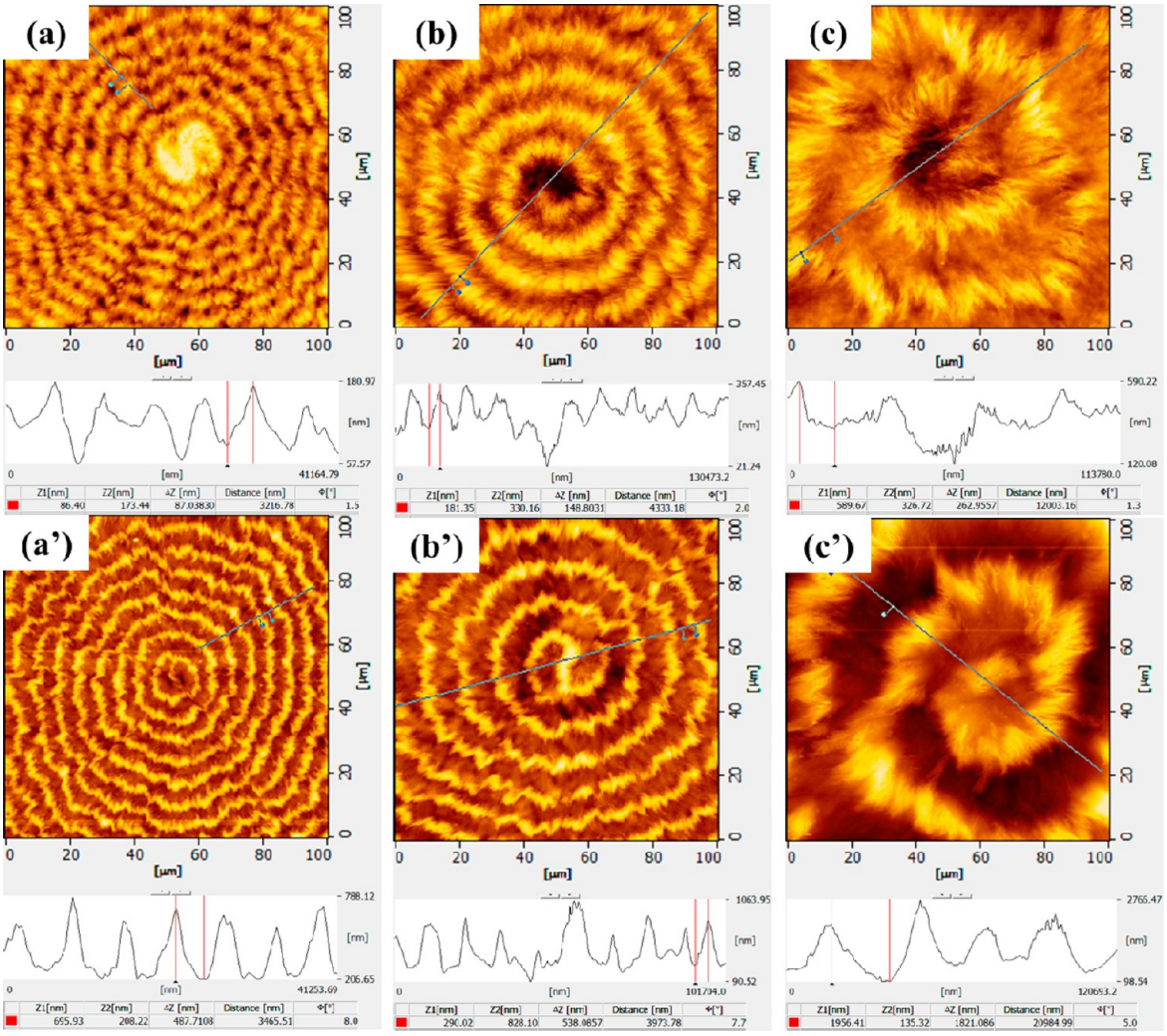

Figure 6. AFM images (topography) of a POM banded spherulite of the POM/PLLA (50/50) samples and the PLLA-etched ones, after isothermal crystallization at various $T_{c,POM}$: (a, a′) 141 °C; (b, b′) 147 °C; (c, c′) 151 °C, respectively.

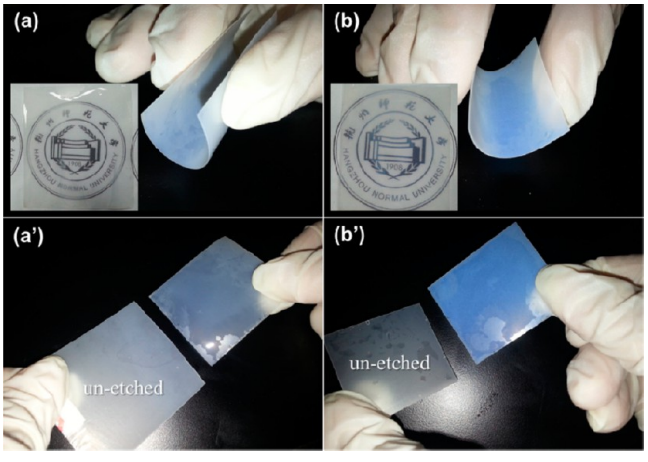

Figure 7. Microscopic images of POM/PLLA (50/50) blend films after etching: (a) quenched and (b) 141 °C-isothermally crystallized samples. Note that the corresponding samples unetched are also exhibited as controllable ones.

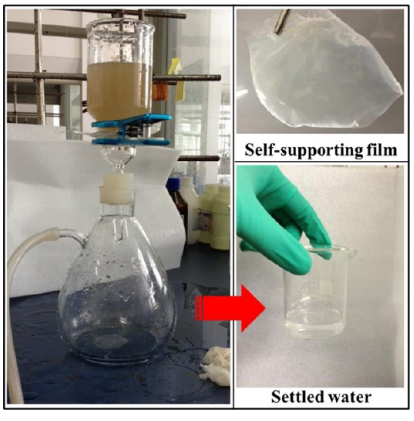

Figure 8. Self-supporting film (prepared by removal of PLLA of the POM/PLLA (50/50) blend) is used as a filtration paper. Note that the POM completely crystallized at 141 °C.

values. For these cases, as illustrated in Scheme 1c, the expelled PLLA chains are distributed into interlamellar and/or interfibrillar regions within POM spherulites. On the one hand, the amorphous PLLA chains lie near the lamellar surfaces might lead to the additional surface stresses and thereby enhance twisting of POM lamellae; on the other hand, the amorphous PLLA chains expelled into interfibrillar areas would make the adjacent lamellae bundled, and therefore lead themselves to be trapped in the "narrow cells" constructed by

DOI: 10.1021/acsami.5b00848
ACS Appl. Mater. Interfaces 2015, 7, 6946−6954

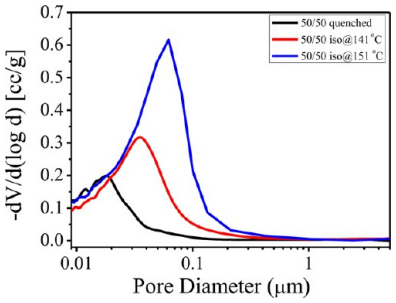

Figure 9. Pore-size distribution porous POM films (from POM/PLLA samples crystallized under various conditions) after removal of PLLA components by solvent etching.

the POM lamellae, as illustrated in Scheme 1d where the details of lamellar twisting and branching are ignored, for simplification. Eventually, accompanied by the twisting of the POM lamellae, these "narrow cells" connect with each other to transform into a continuous phase (that is, the 3D interpenetrated channels after etching). Moreover, the lamellae (fibrils) bundled by the excluded PLLA chains act as junctions within POM spherulites to give the final banded-spherulitic frameworks after etching enough strength for the further application.

Thus, the pore size of the nanoporous POM materials obtained from the isothermally crystallized POM/PLLA blends is strongly influenced by the amorphous layer thickness of POM crystals (l_a) and the space of bands within a spherulite (l). And l, for these cases, is mainly determined by the lamellar twisting ability related to $T_{c,POM}$. The twisting of lamellae is restricted at high temperatures, leading to an increase of l. Moreover, with the elevation of $T_{c,POM}$, l_a would gradually increase, resulting from the increasing segregation of amorphous PLLA chains into the interlamellar and/or interfibrillar regimes due to the depressed branching ability of POM lamellae. So, the amount of amorphous PLLA chains located in the interlamellar and/or interfibrillar areas is dependent on $T_{c,POM}$, and such dependence makes it possible to modulate the pore size of the final nanoporous materials just by adjusting the crystal morphology controlled by T_c. This is further confirmed by the noticeable increase of the difference in height between the "peaks" and "valleys" within a spherulite, as measured by AFM (Figure 6), between before and after etching with the elevating the $T_{c,POM}$.

It should be noted that the strategy for fabricating nanoporous materials would also be applicable for other polymer blends with the interlamellar/interfibrillar structures. The size of such porous materials is close to the meso-/macroporous materials from BCPs but much smaller than the porous materials with submicro-/microscale pores/channels from cocontinuous immiscible polymer blends. On the other hand, the obtained nanoporous materials show nice mechanical properties because of the crystals as the frame network. Finally, the nanoporous materials can be obtained over the large component ratio and the pore structure can be modulated by the component ratios and the crystallization conditions.

5. CONCLUSION

Nanoporous polymeric materials with hierarchical patterned surfaces and 3D interpenetrated internal channels are successfully achieved by using a melt-miscible binary blend. The poorly crystallizable PLLA chains remain amorphous in the miscible POM/PLLA blends and are expelled out from the POM crystals to locate in the interlamellar and/or interfibrillar

Scheme 1. Schematic Illustration of the "Crystallization-Modulated" 3-D Interpenetrated Nanoporous POM Materials[a]

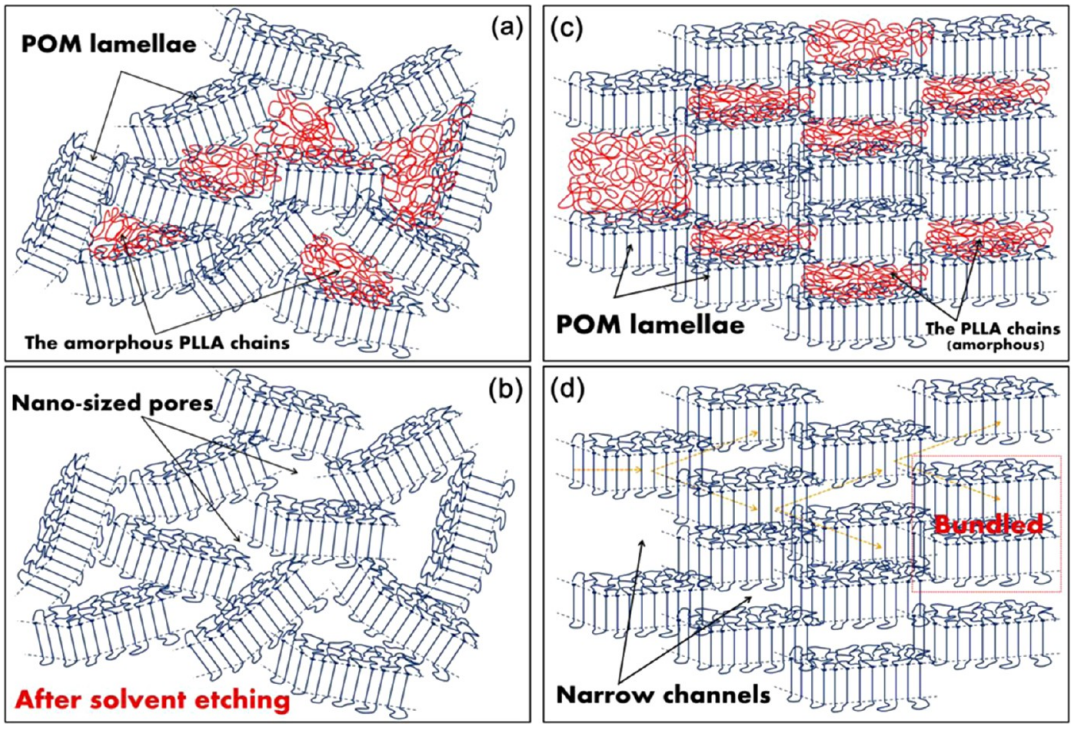

[a]Panels a and c are corresponding to the materials obtained from the quenching and isothermal crystallizing process, respectively. And the corresponding samples after solvent etching are demonstrated in panels b and d.

DOI: 10.1021/acsami.5b00848
ACS Appl. Mater. Interfaces 2015, 7, 6946−6954

regions during the microphase separation induced by crystallization of POM. By isothermal crystallization at various T_c values, in the presence of amorphous PLLA chains, POM crystallizes into banded spherulites, leading to the nanoscaled interlamellar and/or interfibrillar including the amorphous PLLA within POM spherulites. By removal of the amorphous PLLA chains, nanoporous POM materials with 3D interpenetrated channels can be easily obtained. Moreover, the banded-spherulitic frameworks endow the final obtained materials with hierarchical patterned surfaces, which make them much easier for water/aqueous to pass through. Furthermore, the size, structure and organization of pores/channels in the obtained nanoporous POM materials can be manipulated by crystallization conditions. It is expected that the nanoporous materials obtained, especially with hierarchical patterned surfaces, can be applied in various areas, and such a synthetic strategy should be applicable for other melt-miscible binary polymeric blends, therefore, to offer a new path for making nanoporous polymeric materials.

■ ASSOCIATED CONTENT

Supporting Information

WAXD patterns of POM/PLLA blends, relative crystallinity of POM/PLLA blends, PLM images of the crystallized POM/PLLA blends, confined crystallization of PLLA in the POM/PLLA blends, phase images of banded spherulites in PLLA/POM blends, FTIR spectra of neat PLLA, POM, POM/PLLA and PLLA-etched POM/PLLA samples, UV−vis transmittance spectra of porous films obtained from the POM/PLLA blends, pore size, pore volume and surface areas of the porous materials and water contact angle of the porous films obtained from the POM/PLLA blends. This material is available free of charge via the Internet at http://pubs.acs.org.

■ AUTHOR INFORMATION

Corresponding Author

*(Y.L.) E-mail: yongjin-li@hznu.edu.cn. Fax: +86 571 28867899. Telephone: +86 57128867026.

Notes

The authors declare no competing financial interest.

■ ACKNOWLEDGMENTS

This work was financially supported by the National Science Foundation of China (51173036, 21374027) and the Ministry of Education program for New Century Excellent (NCET-13-0762).

■ REFERENCES

(1) Wu, D. C.; Xu, F.; Sun, B.; Fu, R. W.; He, H. K.; Matyjaszewski, K. Design and Preparation of Porous Polymers. *Chem. Rev.* **2012**, *112*, 3959−4015.

(2) Du, N. Y.; Robertson, G. P.; Song, J. S.; Pinnau, I.; Thomas, S.; Guiver, M. D. Polymers of Intrinsic Microporosity Containing Trifluoromethyl and Phenylsulfone Groups as Materials for Membrane Gas Separation. *Macromolecules* **2008**, *41*, 9656−9662.

(3) Furukawa, H.; Yaghi, O. M. Storage of Hydrogen, Methane, and Carbon Dioxide in Highly Porous Covalent Organic Frameworks for Clean Energy Applications. *J. Am. Chem. Soc.* **2009**, *131*, 8875−8883.

(4) Doonan, C. J.; Tranchemontagne, D. J.; Glover, T. G.; Hunt, J. R.; Yaghi, O. M. Exceptional Ammonia Uptake by a Covalent Organic Framework. *Nat. Chem.* **2010**, *2*, 235−238.

(5) Martin, C. F.; Stockel, E.; Clowes, R.; Adams, D. J.; Cooper, A. I.; Pis, J. J.; Rubiera, F.; Pevida, C. Hypercrosslinked Organic Polymer Networks as Potential Adsorbents for Pre-combustion CO_2 Capture. *J. Mater. Chem.* **2011**, *21*, 5475−5483.

(6) Lv, Y. Q.; Hughes, T. C.; Hao, X. J.; Hart, N. K.; Littler, S. W.; Zhang, X. Q.; Tan, T. W. A Novel Route to Prepare Highly Reactive and Versatile Chromatographic Monoliths. *Macromol. Rapid Commun.* **2010**, *31*, 1785−1790.

(7) Zhang, R. Y.; Qi, L.; Xin, P. Y.; Yang, G. L.; Chen, Y. Preparation of Macroporous Monolith with Three Dimensional Bicontinuous Skeleton Structure by Atom Transfer Radical Polymerization for HPLC. *Polymer* **2010**, *51*, 1703−1708.

(8) Pulko, I.; Wall, J.; Krajnc, P.; Cameron, N. R. Ultra-High Surface Area Functional Porous Polymers by Emulsion Templating and Hypercrosslinking: Efficient Nucleophilic Catalyst Supports. *Chem.—Eur. J.* **2010**, *16*, 2350−2354.

(9) Chan-Thaw, C. E.; Villa, A.; Katekomol, P.; Su, D. S.; Thomas, A.; Prati, L. Covalent Triazine Framework as Catalytic Support for Liquid Phase Reaction. *Nano Lett.* **2010**, *10*, 537−541.

(10) Abidian, M. R.; Kim, D. H.; Martin, D. C. Conducting-Polymer Nanotubes for Controlled Drug Release. *Adv. Mater.* **2006**, *18*, 405−409.

(11) Jackson, E. A.; Hillmyer, M. A. Nanoporous Membranes Derived from Block Copolymers: From Drug Delivery to Water Filtration. *ACS Nano* **2010**, *4*, 3548−3553.

(12) Zhao, C.; Danish, E.; Cameron, N. R.; Kataky, R. Emulsion-Templated Porous Materials (PolyHIPEs) for Selective Ion and Molecular Recognition and Transport: Applications in Electrochemical Sensing. *J. Mater. Chem.* **2007**, *17*, 2446−2453.

(13) Haberkorn, N.; Lechmann, M. C.; Sohn, B. H.; Char, K.; Gutmann, J. S.; Theato, P. Templated Organic and Hybrid Materials for Optoelectronic Applications. *Macromol. Rapid Commun.* **2009**, *30*, 1146−1166.

(14) Tseng, W. H.; Chen, C. K.; Chiang, Y. W.; Ho, R. M.; Akasaka, S.; Hasegawa, H. Helical Nanocomposites from Chiral Block Copolymer Templates. *J. Am. Chem. Soc.* **2009**, *131*, 1356−1357.

(15) Crossland, E. J. W.; Kamperman, M.; Nedelcu, M.; Ducati, C.; Wiesner, U.; Smilgies, D. M.; Toombes, G. E. S.; Hillmyer, M. A.; Ludwigs, S.; Steiner, U.; Snaith, H. J. A Bicontinuous Double Gyroid Hybrid Solar Cell. *Nano Lett.* **2008**, *9*, 2807−2812.

(16) Wang, Y.; He, C. C.; Xing, W. H.; Li, F. B.; Tong, L.; Chen, Z. Q.; Liao, X. Z.; Steinhart, M. Nanoporous Metal Membranes with Bicontinuous Morphology from Recyclable Block-Copolymer Templates. *Adv. Mater.* **2010**, *22*, 2068−2072.

(17) McKeown, N. B.; Budd, P. M. Exploitation of Intrinsic Microporosity in Polymer-based Materials. *Macromolecules* **2010**, *43*, 5163−5176.

(18) Holst, J. R.; Cooper, A. I. Ultrahigh Surface Area in Porous Solids. *Adv. Mater.* **2010**, *22*, 5212−5216.

(19) McKeown, N. B.; Budd, P. M. Polymers of Intrinsic Microporosity (PIMs): Organic Materials for, Membrane Separations, Heterogeneous Catalysis and Hydrogen Storage. *Chem. Soc. Rev.* **2006**, *35*, 675−683.

(20) Lu, A. H.; Schüth, F. Nanocasting: A Versatile Strategy for Creating Nanostructured Porous Materials. *Adv. Mater.* **2006**, *18*, 1793−1805.

(21) Thomas, A.; Goettmann, F.; Antonietti, M. Hard Templates for Soft Materials: Creating Nanostructured Organic Materials. *Chem. Mater.* **2008**, *20*, 738−755.

(22) Li, Q.; Retsch, M.; Wang, J.; Knoll, W.; Jonas, U. Porous Networks through Colloidal Templates. *Top. Curr. Chem.* **2009**, *287*, 135−180.

(23) Olson, D. A.; Chen, L.; Hillmyer, M. A. Templating Nanoporous Polymers with Ordered Block Copolymers. *Chem. Mater.* **2007**, *20*, 869−890.

(24) Kim, J. K.; Yang, S. Y.; Lee, Y. M.; Kim, Y. Functional Nanomaterials Based on Block Copolymer Self-Assembly. *Prog. Polym. Sci.* **2010**, *35*, 1325−1349.

(25) Wang, Y.; Li, F. B. An Emerging Pore-Making Strategy: Confined Swelling-Induced Pore Generation in Block Copolymer Materials. *Adv. Mater.* **2011**, *23*, 2134−2148.

DOI: 10.1021/acsami.5b00848
ACS Appl. Mater. Interfaces 2015, 7, 6946−6954

(26) Sarazin, P.; Favis, B. D. Morphology Control in Co-continuous Poly(L-lactide)/Polystyrene Blends: A Route towards Highly Structured and Interconnected Porosity in Poly(L-lactide) Materials. *Biomacromolecules* **2003**, *4*, 1669−1679.
(27) Salehi, P.; Sarazin, P.; Favis, B. D. Porous Devices Derived from Co-continuous Polymer Blends as a Route for Controlled Drug Release. *Biomacromolecules* **2008**, *9*, 1131−1138.
(28) Xiang, Z. Y.; Sarazin, P.; Favis, B. D. Controlling Burst and Final Drug Release Times from Porous Polylactide Devices Derived from Co-continuous Polymer Blends. *Biomacromolecules* **2009**, *10*, 2053−2066.
(29) Jungnickel, B. J. Crystallization Kinetical Peculiarities in Polymer Blends. *Lect. Notes Phys.* **2003**, *606*, 208−237.
(30) Liu, J. P.; Jungnickel, B. J. Crystallization Kinetical and Morphological Peculiarities in Binary Crystalline/Crystalline Polymer Blends. *J. Polym. Sci. Part B.: Polym. Phys.* **2007**, *45*, 1917−1931.
(31) Chen, H. L.; Liu, H. H.; Lin, J. S. Microstructure of Semicrystalline Poly(L-lactide)/Poly(4-vinylphenol) Blends Evaluated from SAXS Absolute Intensity Measurement. *Macromolecules* **2000**, *33*, 4856−4860.
(32) Chuang, W. T.; Jeng, U. S.; Sheu, H. S.; Hong, P. D. Competition between Phase Separation and Crystallization in a PCL/PEG Polymer Blend Captured by Synchronized SAXS, WAXS, and DSC. *Macromol. Res.* **2006**, *14*, 45−51.
(33) Chuang, W. T.; Jeng, U. S.; Hong, P. D.; Sheu, H. S.; Lai, Y. H.; Shih, K. S. Dynamic Interplay between Phase Separation and Crystallization in a Poly(ε-caprolactone)/Poly(ethylene glycol) Oligomer Blend. *Polymer* **2007**, *48*, 2919−2927.
(34) Keith, H. D.; Padden, F. J., Jr.; Russell, T. P. Morphological Changes in Polyesters and Polyamides Induced by Blending with Small Concentrations of Polymer Diluents. *Macromolecules* **1989**, *22*, 666−675.
(35) Toda, A.; Taguchi, K.; Kajioka, H. Growth of Banded Spherulites of Poly(ε-caprolactone) from the Blends: An Examination of the Modeling of Spherulitic Growth. *Polymer* **2012**, *53*, 1765−1771.
(36) He, Z. Y.; Liang, Y. R.; Han, C. C. Confined Nucleation and Growth of Poly(ethylene oxide) on the Different Crystalline Morphology of Poly(butylene succinate) From a Miscible Blend. *Macromolecules* **2013**, *46*, 8264−8274.
(37) Höglund, A.; Odelius, K.; Albertsson, A. C. Crucial Differences in the Hydrolytic Degradation between Industrial Polylactide and Laboratory-Scale Poly(L-lactide). *ACS Appl. Mater. Interfaces* **2012**, *4*, 2788−2793.
(38) Washburn, E. W. The Dynamics of Capillary Flow. *Phys. Rev.* **1921**, *17*, 273−283.
(39) Qiu, J. S.; Xing, C. Y.; Cao, X. J.; Wang, H. T.; Wang, L.; Zhao, L. P.; Li, Y. J. Miscibility and Double Glass Transition Temperature Depression of Poly(L-lactic acid) (PLLA)/Poly(oxymethylene) (POM) Blends. *Macromolecules* **2013**, *46*, 5806−5814.
(40) Qiu, J. S.; Guan, J. P.; Wang, H. T.; Zhu, S. S.; Cao, X. J.; Ye, Q. L.; Li, Y. J. Enhanced Crystallization Rate of Poly(L-lactic acid) (PLLA) by Polyoxymethylene (POM) Fragment Crystals in the PLLA/POM Blends with a Small Amount of POM. *J. Phys. Chem. B* **2014**, *118*, 7167−7176.
(41) Keller, A. The Spherulitic Structure of Crystalline Polymers. Part II. The Problem of Molecular Orientation in Polymer Spherulites. *J. Polym. Sci.* **1955**, *17*, 351−364.
(42) Keith, H. D.; Padden, F. J., Jr. The Optical Behavior of Spherulites in Crystalline Polymers. Part I. Calculation of Theoretical Extinction Patterns in Spherulites with Twisting Crystalline Orientation. *J. Polym. Sci.* **1959**, *39*, 101−122.
(43) Keith, H. D.; Padden, F. J., Jr. The Optical Behavior of Spherulites in Crystalline Polymers. Part II. The Growth and Structure of the Spherulites. *J. Polym. Sci.* **1959**, *39*, 123−138.
(44) Price, F. P. On Extinction Patterns of Polymer Spherulites. *J. Polym. Sci.* **1959**, *39*, 139−150.
(45) Keller, A. Investigations on Banded Spherulites. *J. Polym. Sci.* **1959**, *39*, 151−173.
(46) Fujiwara, Y. The Superstructure of Melt-Crystallized Polyethylene. I. Screwlike Orientation of Unit Cell in Polyethylene Spherulites with Periodic Extinction Rings. *J. Appl. Polym. Sci.* **1960**, *4*, 10−15.
(47) Keith, H. D.; Padden, F. J., Jr. Twisting Orientation and the Role of Transient States in Polymer Crystallization. *Polymer* **1984**, *25*, 28−42.
(48) Keith, H. D.; Padden, F. J., Jr. Banding in Polyethylene and Other Spherulites. *Macromolecules* **1996**, *29*, 7776−7786.
(49) Keith, H. D. Banding in Spherulites: Two Recurring Topics. *Polymer* **2001**, *42*, 9987−9993.
(50) Eshelby, J. D. Screw Dislocations in Thin Rods. *J. Appl. Phys.* **1953**, *24*, 176−179.
(51) Schultz, J. M.; Kinloch, D. R. Transverse Screw Dislocations: A Source of Twist in Crystalline Polymer Ribbons. *Polymer* **1969**, *10*, 271−278.
(52) Schultz, J. M. Self-Induced Field Model for Crystal Twisting in Spherulites. *Polymer* **2003**, *44*, 433−441.
(53) Okano, K. Note on the Lamellar Twist is Polymer Spherulites. *Jpn. J. Appl. Phys.* **1964**, *3*, 351−353.
(54) Xu, J.; Guo, B. H.; Zhang, Z. M.; Zhou, J. J.; Jiang, Y.; Yan, S. K.; Li, L.; Wu, Q.; Chen, G. Q.; Schultz, J. M. Direct AFM Observation of Crystal Twisting and Organization in Banded Spherulites of Chiral Poly(3-hydroxybutyrate-co-3-hydroxyhexanoate). *Macromolecules* **2004**, *37*, 4118−4123.
(55) Woo, E. M.; Chang, C. S.; Wu, M. C. A New Crystal Morphology of Straight-Stalk Dendrites in Blends of Poly(butylene adipate) with Amorphous Poly(vinyl acetate). *Mater. Lett.* **2007**, *61*, 3542−3546.
(56) Chen, Y. F.; Woo, E. M. Growth Regimes and Spherulites in Thin-Film Poly(ε-caprolactone) with Amorphous Polymers. *Colloid Polym. Sci.* **2008**, *286*, 917−926.
(57) Schultz, J. M. Self-Generated Fields and Polymer Crystallization. *Macromolecules* **2012**, *45*, 6299−6323.
(58) Ye, L. J.; Qiu, J. S.; Wu, T.; Shi, X. C.; Li, Y. J. Banded Spherulite Templated Three-Dimensional Interpenetrated Nanoporous Materials. *RSC Adv.* **2014**, *4*, 43351−43356.

DOI: 10.1021/acsami.5b00848
ACS Appl. Mater. Interfaces 2015, 7, 6946−6954